RESEARCH ARTICLE

Fate map of *Medicago truncatula* root nodules

Ting Ting Xiao[1], Stefan Schilderink[1], Sjef Moling[1], Eva E. Deinum[1,2,*], Eva Kondorosi[3], Henk Franssen[1], Olga Kulikova[1], Andreas Niebel[4,5] and Ton Bisseling[1,6,‡]

ABSTRACT

Legume root nodules are induced by N-fixing rhizobium bacteria that are hosted in an intracellular manner. These nodules are formed by reprogramming differentiated root cells. The model legume *Medicago truncatula* forms indeterminate nodules with a meristem at their apex. This organ grows by the activity of the meristem that adds cells to the different nodule tissues. In *Medicago sativa* it has been shown that the nodule meristem is derived from the root middle cortex. During nodule initiation, inner cortical cells and pericycle cells are also mitotically activated. However, whether and how these cells contribute to the mature nodule has not been studied. Here, we produce a nodule fate map that precisely describes the origin of the different nodule tissues based on sequential longitudinal sections and on the use of marker genes that allow the distinction of cells originating from different root tissues. We show that nodule meristem originates from the third cortical layer, while several cell layers of the base of the nodule are directly formed from cells of the inner cortical layers, root endodermis and pericycle. The latter two differentiate into the uninfected tissues that are located at the base of the mature nodule, whereas the cells derived from the inner cortical cell layers form about eight cell layers of infected cells. This nodule fate map has then been used to re-analyse several mutant nodule phenotypes. This showed, among other things, that intracellular release of rhizobia in primordium cells and meristem daughter cells are regulated in a different manner.

KEY WORDS: Medicago, Indeterminate root nodule, Nodule primordium, Nodule meristem, Endodermis, Inner cortex

INTRODUCTION

The symbiosis of rhizobium and legumes results in the formation of N-fixing root nodules, which can have determinate or indeterminate growth. Determinate nodules lose their meristem at an early stage of development. By contrast, indeterminate legume nodules have a persistent meristem at their apices by which they add cells to the different nodule tissues throughout their lifetime (Hadri et al., 1998). The model legume *Medicago truncatula* (Medicago) forms indeterminate nodules, so their nodule tissues are of graded age with

the youngest cells near the meristem. The central tissue of the nodule is composed of two cell types: the infected cells that harbour the rhizobia, interspersed with specialized uninfected cells. This central tissue is surrounded by three uninfected peripheral tissues: the nodule parenchyma, endodermis and cortex (Bond, 1948; Van de Wiel et al., 1990; Brewin, 1991). Uninfected tissues are also present at the basal part of the nodule (see Fig. 7A).

In general, it is assumed that in indeterminate nodules, the cells along the complete apical-basal axis are derived from the apical meristem. However, this assumption creates some paradoxes. For example, how can the uninfected tissues at the basal part of the nodule be formed from the meristem and not be infected by rhizobium, whereas the layers that are subsequently formed do become infected? Furthermore, the *nf-ya1* mutant forms nodules lacking a meristem or have a meristem that gives rise to daughter cells in which intracellular infection is blocked. However, several cell layers with fully infected cells are present at the base of these nodules (Combier et al., 2006; Laporte et al., 2014).

Root nodule formation is initiated by mitotic activation of root cells. The most detailed analysis of which root tissue cells are activated has been performed on *Medicago sativa* (Timmers et al., 1999). This study showed that inner and middle cortical cells, as well as pericycle cells, become mitotically active upon rhizobial inoculation. Furthermore, it was shown that the cells of the middle cortex form the nodule meristem. However, whether cells derived from the inner cortex and pericycle contribute to the mature nodule has not been studied. Based on the mutant nodule phenotype of *nf-ya1-1*, we hypothesize that cells derived from inner cortex form several cell layers of infected cells at the base of the nodule and intracellular infection of these cells is less strictly controlled than infection of cells derived from nodule meristem. To test this hypothesis, we selected Medicago (*M. truncatula* A17) to generate a detailed nodule fate map.

The infection process in Medicago starts with the formation of an infection thread in a root hair and it grows to the base of the infected root hair cell. Subsequently, infection threads traverse outer cortical cells, allowing rhizobia to reach the dividing cortical cells. This cluster of dividing cells is named nodule primordium and at its apex a meristem is formed (Libbenga and Harkes, 1973; Yang et al., 1994). Infection threads penetrate host cells derived from the meristem and rhizobia are internalised. During this release from infection threads, rhizobia become surrounded by the host membrane, a process controlled by a specific exocytotic pathway (Ivanov et al., 2012), leading to the formation of nitrogen-fixing symbiosomes (Roth and Stacey, 1989; Brewin, 2004). Symbiosomes then divide, differentiate and ultimately fill the infected cells.

Nodule formation as well as the infection process are controlled by specific lipochito-oligosaccharides (Nod factors) that are secreted by rhizobia (Lerouge et al., 1990). Nod factors mitotically activate root cells and form a nodule primordium (Bond, 1948; Nutman, 1948; Libbenga and Harkes, 1973; Lancelle

[1]Department of Plant Sciences, Laboratory of Molecular Biology, Wageningen University, Droevendaalsesteeg 1, Wageningen 6708 PB, The Netherlands. [2]Department of Systems Biophysics, FOM institute AMOLF, Science Park 104, Amsterdam 1098 XG, The Netherlands. [3]Institute of Biochemistry, Biological Research Centre, Hungarian Academy of Sciences, Szeged 6726, Hungary. [4]INRA, Laboratoire des Interactions Plantes-Microorganismes (LIPM), UMR441, Castanet-Tolosan F-31326, France. [5]CNRS, Laboratoire des Interactions Plantes-Microorganismes (LIPM), UMR2594, Castanet-Tolosan F-31326, France. [6]College of Science, King Saud University, Post Office Box 2455, Riyadh 11451, Saudi Arabia.
*Present address: Institute of Evolutionary Biology, The University of Edinburgh, Edinburgh, UK.

‡Author for correspondence (ton.bisseling@wur.nl)

and Torrey, 1985; Dudley et al., 1987; Nap and Bisseling, 1990; Brewin, 1991; Yang et al., 1994; Timmers et al., 1999). However, the difference between a primordium and a young nodule is not well defined.

Our fate map studies confirmed that, in Medicago, as in *M. sativa*, the inner and middle cortical and pericycle cells are mitotically activated upon rhizobium infection and the nodule meristem is derived from the middle cortex (Timmers et al., 1999). We have, in addition, established that the first and second cortical layers have only a limited role in nodule ontogeny, that the third cortical layer gives rise to the nodule meristem and about eight cell layers with fully infected cells at the base of the central tissue are derived from the inner cortex (4th and 5th cortical layer). Furthermore, cell divisions are also induced in the root endodermis and the endodermis/pericycle-derived cells form the uninfected cell layers at the base of the nodule. Using this nodule fate map, we re-analysed several Medicago mutants.

RESULTS AND DISCUSSION
Pericycle, endodermis and cortical layers contribute to the Medicago nodule primordium

Medicago roots have in general five cortical cell layers, although roots with four and six layers also occur. We refer to the outermost layer as C1 and the inner most layer as C5. The inner most cortical cells are about 15 μm thick, whereas the cells of the other four cortical layers are about twice as thick (30 μm). The epidermis, endodermis and pericycle each contain a single cell layer (Fig. 1A).

To determine which cell layers of the root contribute to the formation of a nodule primordium, Medicago seedlings were inoculated with *S. meliloti 2011* and root segments were collected at different time points 1-5 days after inoculation. These were fixed

and embedded in Technovit 7100. Longitudinal sections of about 50 root segments were made and analysed by light microscopy. Based on these analyses, we divided nodule development into six stages (Fig. 1). At stage I (Fig. 1A), anticlinal divisions are induced in the pericycle. This is rapidly followed by anticlinal divisions first in C5 and slightly later in C4 (stage II) (Fig. 1B). During stage III (Fig. 1C), periclinal divisions are induced in C5 and C4, and anticlinal divisions occur in C3 and endodermis. At stage IV (Fig. 1D), periclinal divisions occur in C3, pericycle and endodermis; cell divisions continued in C4 and C5; and some anticlinal divisions are induced in C2. At stage V (Fig. 1E), C3-derived cells have formed a multi-layered (future) meristem, C4/5 have formed about eight cell layers, and the endodermis and pericycle have formed six to eight cell layers. At this stage of nodule development, mitotic activity in the non-meristematic (C4/5) cells stops. These cells start to enlarge and are penetrated by infection threads. These characteristics distinguish them morphologically from the (future) meristem cells (C3), which are small and not infected. At stage V it still can be traced from which root cell layers the primordium cells are derived. At stage VI (Fig. 1F) this is not always possible due to the formation of peripheral tissues, but meristem and C4/5-derived cells can be recognized based on their distinguishing morphological characteristics. At stage VI, vascular bundles are established at the periphery. Furthermore, the meristem starts now to add cells to the nodule tissues; this is why we named it (future) meristem at stage V. We propose to name the clusters of cells a nodule primordium up to stage V and nodule from stage VI onwards. Previously, it was proposed that the clusters of dividing cells at stages I and II be called an initial primordium (Timmers et al., 1999). However, as these cells become part of the mature nodule (see below), we will use the term nodule primordium.
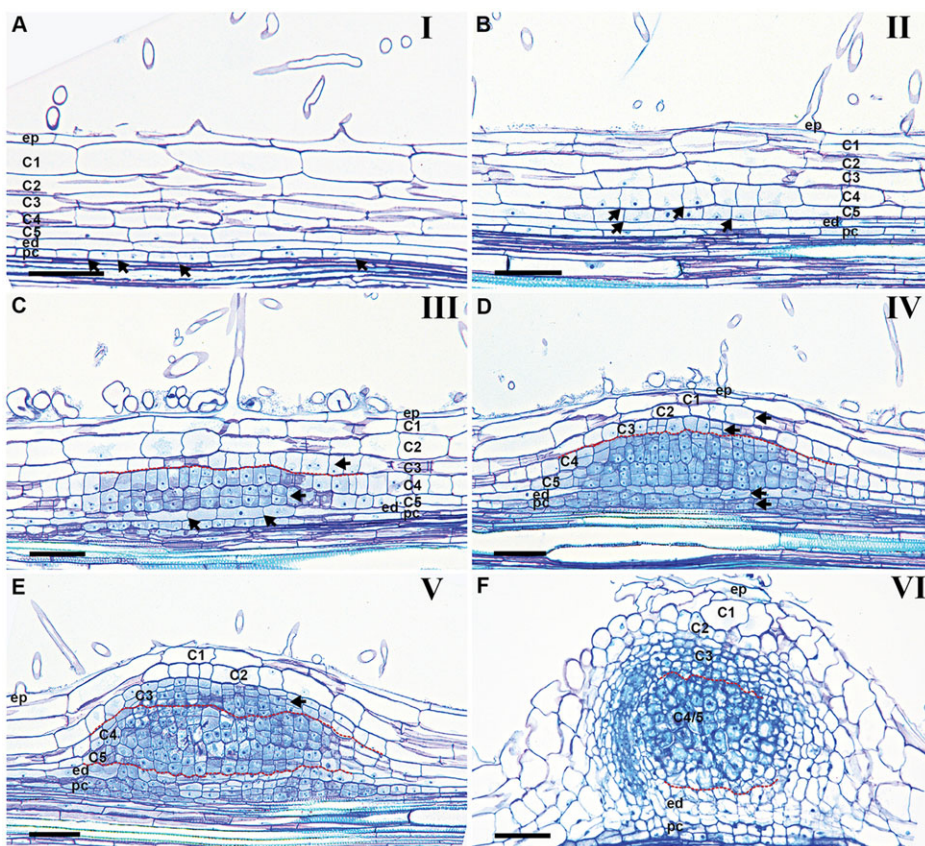

Fig. 1. Medicago nodule primordia at subsequent stages of development. Longitudinal sections of Medicago root segments. (A) Stage I. Anticlinal cell divisions are induced in the pericycle (arrows) and occasionally occur in C5 and C4. (B) Stage II. Cell divisions (anticlinal) extend to C5 and C4 (arrows); anticlinal divisions occasionally occur in C3. The higher frequency of divisions in the inner layers reflects that the divisions start from there. (C) Stage III. Anticlinal divisions occur in C3 (arrow) and endodermis (arrows); periclinal divisions are induced in C4/5-derived cells (arrow); anticlinal cell divisions occasionally occur in C2. (D) Stage IV. Periclinal cell divisions are induced in C3 (arrow), endodermis (arrow) and pericycle (arrow); C4/5 cell division continue; anticlinal cell divisions occur in C2 (arrow). (E) Stage V. C3-derived cells form multiple cell layers (arrow); C4/5 form about eight cell layers; pericycle and endodermis contribute about six cell layers to the basal part of the primordium; C2 and C1 have divided a few times anticlinally. (F) Stage VI. Vascular bundles are formed at the periphery of the primordia; meristem starts functioning. From this moment onwards, a nodule primordium become a nodule. In C-F, a red line indicates the border between cells derived from C3, C4/5 and endodermis. ep, epidermis; C1, 1st cortical cell layer; C2, 2nd cortical cell layer; C3, 3rd cortical cell layer; C4, 4th cortical cell layer; C5, 5th cortical cell layer; ed, endodermis; pc, pericycle. Scale bars: 75 μm.

To obtain better insight into the timing of the different stages of nodule primordium formation, we also spot inoculated Medicago roots with *S. meliloti*. Stage I starts at about 24 h post-inoculation (hpi), stage II at 27-33 hpi, stage III at 33-35 hpi, stage IV at 42-48 hpi, stage V at 65-70 hpi and stage VI after 80 hpi.

Medicago lateral root formation also starts with divisions in the pericycle, endodermis and cortex cells (Op den Camp et al., 2011; Herrbach et al., 2014), which is very similar to nodule primordium initiation. To distinguish a young lateral root primordium from an early stage (I-III) nodule primordium, we made use of transgenic Medicago roots expressing *MtENOD40::GUS*. This reporter is strongly induced in rhizobium-activated pericycle, endodermis, cortical cells and vascular tissue, and markedly less and restricted in pericycle and vascular tissues of the lateral root primordia (Fig. 2). At stage I a marker like MtENOD40 is essential to distinguish lateral root and nodule primordia. However, at later stages this is not essential as in nodule primordia the frequency of divisions is highest in cortical layers, whereas in lateral root primordia mitotic activity is higher in pericycle and endodermis (T.T.X., unpublished).

We showed that, in Medicago, the mitotic activation of root cells by rhizobium starts in the pericycle and extends outwards to the cortical cell layers. The middle cortical cell layer (C3) ultimately forms the nodule meristem. This is similar to nodule primordium initiation in *M. sativa* (Timmers et al., 1999). In addition, we showed that the endodermis also divides and, together with pericycle and inner cortex cell layers (C4/5), contributes about 16 cell layers to the nodule primordium. Based on these observations, we addressed the issue of whether primordium cells that originate from pericycle up to C4 contribute to mature nodule tissues.

Do primordium cells derived from C4/5 become part of the mature nodule?

First, we determined whether rhizobia can infect C4/5-derived cells. Serial sections of 30 primordia at stage III-IV were analysed. In five primordia (stage III), the infection thread was still in C1 or C2; in 10 (stage III) primordia, the infection thread had just reached C3 (Fig. 3A). In 15 primordia, the infection thread was present in cells derived from C4/5 (Fig. 3B). In 10 of these 15 primordia, C3 cells had divided several times, including both anticlinal and periclinal divisions (stage IV). Therefore, it is likely that cells derived from C3 can still be penetrated by an infection thread after the first anticlinal divisions (stage III). As nodule meristematic cells are not penetrated by infection threads, it is probable that infection threads have to reach C4/5-derived cells before stage IV, i.e. before periclinal divisions are initiated in the C3 layer.

To determine the timing of the infection of the primordium more precisely, spot-inoculated Medicago roots were analysed. At 42-48 hpi, the infection thread had reached C4/5-derived cells (stage IV). Around 80 hpi (stage VI), bacterial release had taken place in cells derived from C4/5 (Fig. 3C,D). This means that release occurs about 32 h after the infection thread reached the primordium cells.

C4/5-derived cells that are infected by rhizobia develop into large infected cells. Therefore, in a mature nodule, about eight cell layers of the central tissue directly developed from C4/5-derived cells and not from the meristem (C3).

Do primordium cells derived from pericycle/endodermis become part of the mature nodule?

The analysis of nodule primordia showed that C4/5-derived cells can be infected by rhizobia. However, whether endodermis- and pericycle-derived cells may also become infected cannot be excluded. In order to trace primordium cells derived from endodermis and pericycle more precisely, we made use of *CASP1*, an *Arabidopsis* gene that is specifically expressed in the root endodermis. It encodes a transmembrane protein that is involved in the formation of casparian strips (Roppolo et al., 2011). To determine whether this gene can be used as an endodermis marker in Medicago, we transformed Medicago roots with *AtCASP1::GUS* (Vermeer et al., 2014) and showed that this construct is expressed in endodermis and also in pericycle, but at low levels (Fig. 4A).

In general, it is presumed that root cells that are mitotically activated are completely de-differentiated. Therefore, we expected that *AtCASP1::GUS* would be repressed when cell divisions are induced in the endodermis. However, when the endodermis had undergone several periclinal as well as anticlinal divisions, all endodermis-derived cells displayed GUS activity. Therefore, we were able to trace endodermal cells during the formation of a nodule primordium and could distinguish them from cortex-derived cells (Fig. 4B). The intensity of the signal in the endodermis-derived cells is (at least) as high as in the endodermis before division. Thus, it is not simply caused by a dilution of GUS present in the root endodermis and the *AtCASP1* promoter must have remained active during endodermal cell divisions. Analyses of serial sections of 30 stage IV-V primordia showed that infection threads do not penetrate endodermis- and pericycle-derived cells, in contrast to C4/5-derived cells. For that reason, the origin of the primordial cells appears to determine whether they can be penetrated by an infection thread or not.

At stage VI the expression of *AtCASP1::GUS* is repressed in most of the endodermis-derived cells and becomes restricted to a single cell layer. Furthermore, it is induced in vascular endodermis (Fig. 4C).
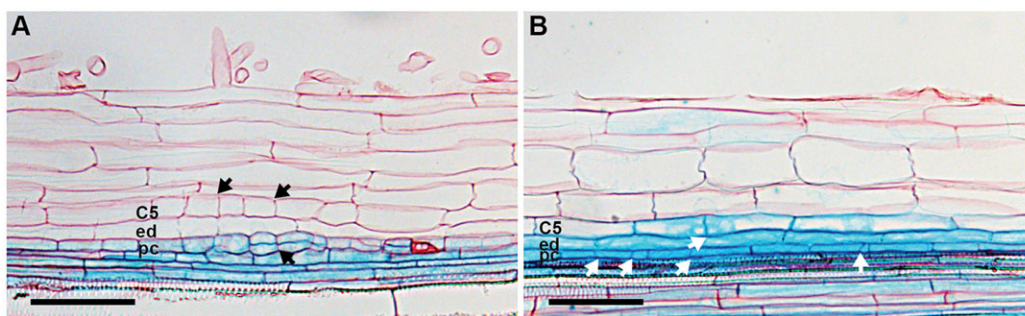

Fig. 2. *MtENOD40::GUS* is a marker to distinguish between early lateral root primordium and nodule primordium. The root (A) and nodule (B) primordia are initiated on the same *MtENOD40::GUS* transgenic root. Primordial, C5 and pericycle cells have divided (black and white arrows); *MtENOD40* is expressed at markedly higher levels in the nodule primordium (B). Scale bars: 75 µm.
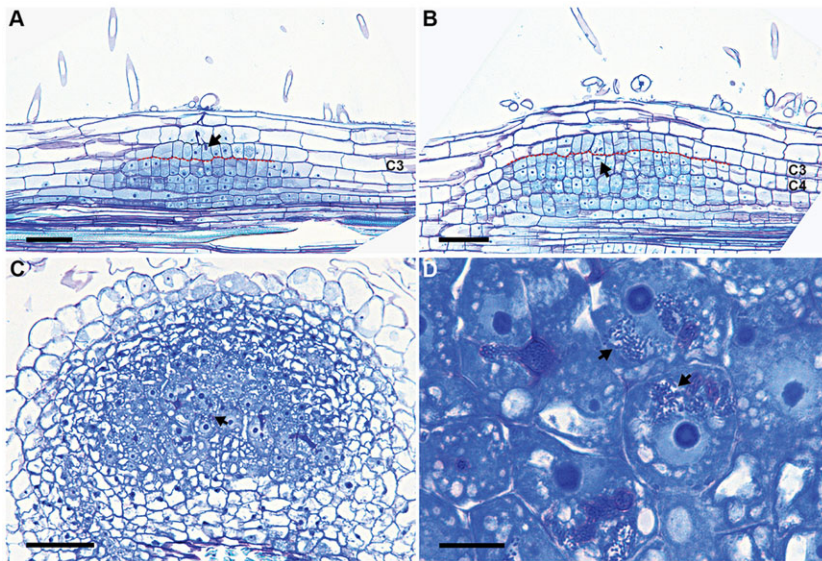
Fig. 3. Infection threads reach C4/5-derived cells before stage IV. (A) At stage III of primordium development, anticlinal divisions are induced in C3 and the tip of the infection thread (arrow) reached C3. (B) At stage IV, the tip of the infection thread has reached the cells derived from C4/5 (arrow). (C) At stage VI (80 hpi), rhizobia (arrow) are released in C4/5-derived cells. (D) Magnification of C shows the released rhizobia (arrows). In A and B, a red line indicates the border between cells derived from C3 and C4. Scale bars: 75 µm in A-C; 10 µm in D.

The maintenance of endodermal-specific gene expression in nodule primordia is also illustrated by the expression of *Scarecrow* (*SCR*). *Arabidopsis* SCR is a GRAS-type transcription factor that is specifically expressed in the root endodermis and is essential for the formation of this tissue (Di Laurenzio et al., 1996). *AtSCR::GUS* is also specifically expressed in the endodermis of transgenic Medicago roots (supplementary material Fig. S1A). Like *AtCASP1*, it remains active in divided endodermal cells in a nodule primordium up to the stage when vascular bundles start to be formed (supplementary material Fig. S1B). It is also activated in cells around the vasculature (supplementary material Fig. S1C).

So, *AtCASP1* and *AtSCR* promoters are expressed in the root endodermis and remain active when cell division is induced. Therefore, we studied whether casparian strips, the hallmark of endodermal cells, are formed in the dividing endodermis cells (Fig. 5). Casparian strips are present in the Medicago root endodermis (Fig. 5A), but upon the first divisions induced by rhizobium, these are lost (Fig. 5B). They are again formed in the single cell layer at the base of the nodule, where expression of *AtCASP1::GUS* is maintained (Fig. 5C). *AtCASP1::GUS* is also expressed in the endodermis around the nodule vascular bundles, and there casparian strips are present (Fig. 5D; supplementary material Fig. S2). By contrast, *AtCASP1::GUS* is not expressed in the nodule endodermis and casparian strips are not formed (Fig. 5D; supplementary material Fig. S2). A 'real' endodermis is only formed at the base of the nodule and around nodule vascular bundles. The fact that the casparian strips are removed before cell division is induced could be a reason why induction of mitotic activity in this tissue is slightly delayed compared with C4/5 cells.

These results show that primordium cells derived from pericycle and endodermis, in contrast to those with a cortical origin, cannot be infected by rhizobia. As the endodermis-derived primordium cells maintain expression of endodermal genes, it is most likely that these cells do not completely de-differentiate, but switch from one differentiated cell type into another, a process known as trans-differentiation (Sugimoto et al., 2011). By which mechanism infection in these endodermis derived cells is prohibited is unclear.
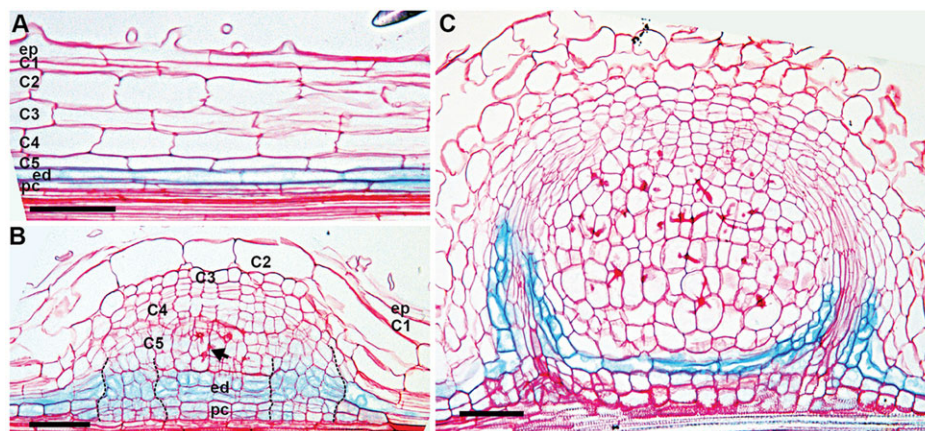

Fig. 4. Endodermis- and pericycle-derived cells of the primordium are not infected. *AtCASP1::GUS* (A) is specifically expressed in the Medicago root endodermis and also in the pericycle but at low levels. *AtCASP1::GUS* (B) remains in endodermis-derived cells at stage IV. Cells at the periphery (indicated in between black lines) will differentiate into nodule parenchyma, including vascular bundles and endodermis. These cells show a different division pattern from their neighbouring cells, which are derived from the same tissue. Infection threads (arrow) never reach endodermis- and pericycle-derived cells. (C) At stage VI, *AtCASP1::GUS* expression is restricted to a single cell layer surrounding the nodule vascular bundle (endodermis). Scale bars: 75 µm.
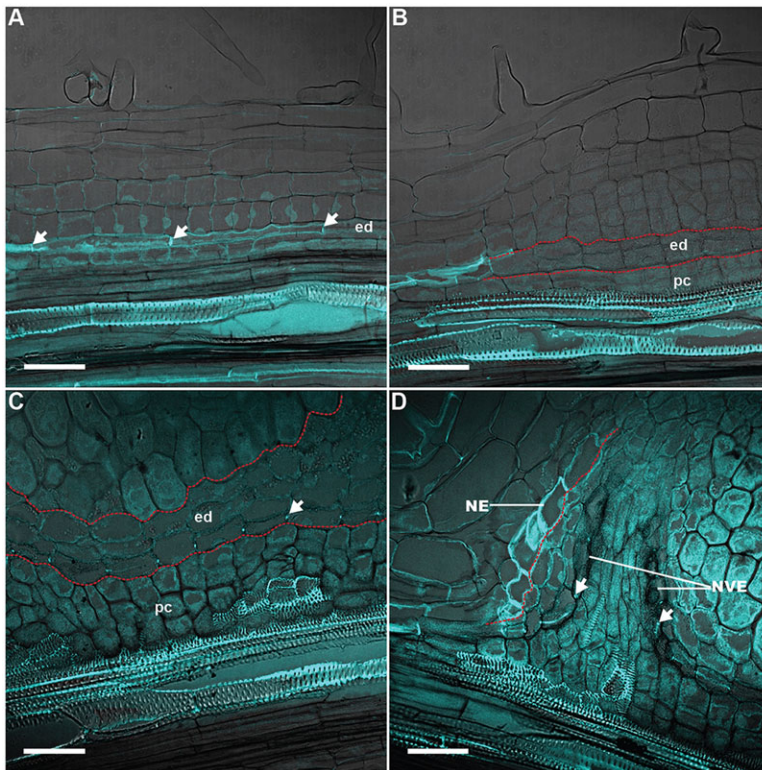
Fig. 5. Casparian strips disappear in the dividing endodermis of nodule primordium. (A) Casparian strips (arrows) in the root endodermis. (B) Casparian strips are absent in dividing endodermal cells. (C) At stage VI, casparian strips (arrow) are formed in the single cell layer at the base of which *AtCASP1* are expressed. (D) Casparian strips (arrows) are formed in the endodermis of nodule vascular bundles but not in the nodule endodermis (split channels in supplementary material Fig. S2). In B and C, red lines indicate the border between cells derived from endodermis and C5 or pericycle, respectively; in D, a red line indicates the border between nodule endodermis and nodule parenchyma. Casparian strips are detected as autofluorescence under UV light. NVE, nodule vascular endodermis; NE, nodule endodermis; ed, epidermis; pc, pericycle. Scale bars: 50 µm.

We hypothesise that the (partial) maintenance of the endodermal fate can contribute to this.

In primordia, infection threads are restricted to the central region of the C4/5-derived cells (Fig. 4B; supplementary material Fig. S1B). At the transition from stage V to VI, the peripheral tissues and vascular bundles start to be formed. These are cells derived from the periphery of the nodule primordium, which includes cells derived from C4, C5, endodermis and pericycle (Fig. 4B; supplementary material Fig. S1B). In nodules, the pericycle- and endodermis-derived cells form the peripheral tissues at the base of the nodule. These are the nodule parenchyma and the few cell layers that are adjacent to the root vascular bundle. In between these two tissues an endodermis containing casparian strips is present.

Markers to distinguish C4/5-derived cells and meristem
We searched for molecular markers enabling us to distinguish between C4/5-derived cells and (future) meristem cells. Infected cells in the infection zone of a mature nodule undergo endoreduplication. Therefore, we expected that C4/5-derived cells enter endoreduplication when they stop dividing (stage V or VI). In this case, markers for mitosis and endoreduplication could be used to distinguish these cells from (future) meristem cells. To identify mitotically active and endoreduplicating cells we used Medicago lines containing an *Arabidopsis* Cyclin B1 reporter (*AtCyclB1.1::GUS*), which is active during mitosis, and *MtCCS52A::GUS*, which is expressed in endoreduplicating cells (Vinardell et al., 2003). *AtCyclB1.1* is active in (future) meristem and not in C4/5-derived cells at stage V and later stages (Fig. 6A). The endoreduplication reporter is not expressed in nodule primordia before stage V and has an expression pattern that is complementary to that of *AtCyclB1* at stage VI; when the latter is switched off in the C4/5-derived cells, *MtCCS52A::GUS* is switched on in these cells (Fig. 6B).

We also tested whether the nodule-specific remorin (*Mt*SYMREM1) that is involved in bacterial release (Lefebvre et al., 2010) can be an extra marker. *MtSYMREM1::GUS* is first induced in
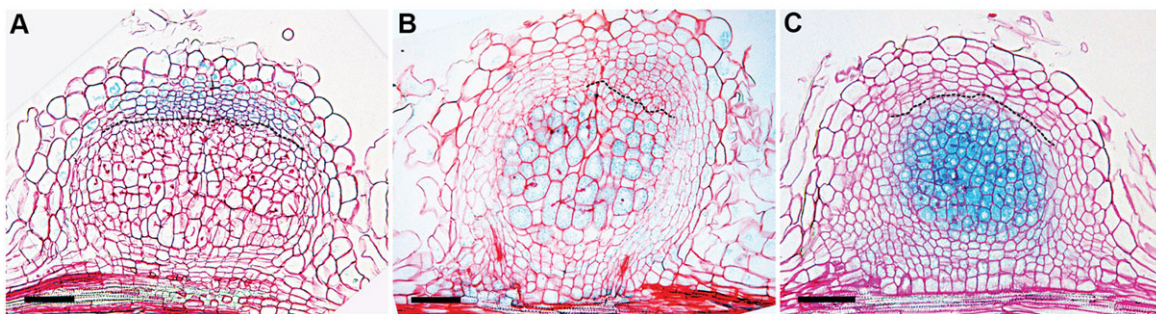

Fig. 6. Molecular markers to distinguish C4/5-derived cells from the nodule meristem (C3). (A) At stage VI, *AtCyclB1.1::GUS* is expressed in C3-derived cells, but not in C4/5-derived cells. (B) At stage VI, the cell endoreduplication marker *MtCCS52A::GUS* is expressed in C4/5-derived cells and in some C1/2 and epidermis-derived cells, but not in C3-derived cells. (C) In transition from stage V to VI, *MtSYMREM1::GUS* is detected in C4/5-derived cells. A black line indicates the border between cells derived from C3 and C4. Scale bars: 75 µm.
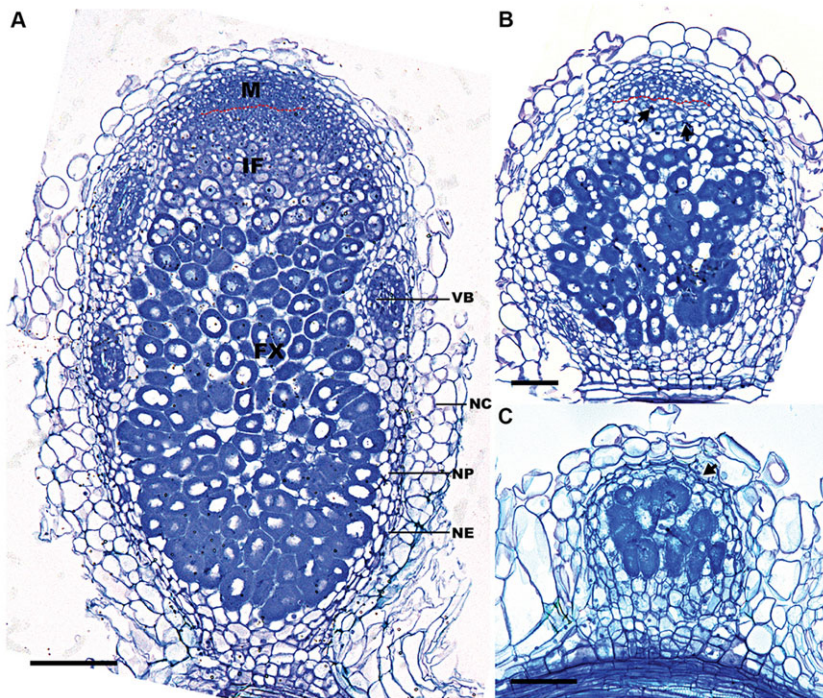
Fig. 7. Mutant *nf-ya1-1* forms nodules with a small nodule meristem or no nodule meristem. Two-week-old wild-type (A) and *nf-ya1-1* (B,C) nodules have a central part well infected by rhizobia. (B) A relatively large *nf-ya1-1* nodule has a small nodule meristem (infection threads are indicated by arrows). (C) A small *nf-ya1-1* nodule does not have a nodule meristem and develops closed nodule endodermis (arrow). M, meristem; IF, infection zone; FX, fixation zone; VB, vascular bundle; NP, nodule parenchyma; NC, nodule cortex; NE, nodule endodermis. In A and B, a red line indicates the border between nodule meristem and infection zone. Scale bars: 75 µm.

C4/5-derived cells and it is not active in cells derived from C3 at stage V/VI (Fig. 6C). We thus have identified three markers allow to distinguish between C4/5- and C3-derived cells at stage V/VI.

DISCUSSION
Analyses of symbiotic mutants
To illustrate the value of our Medicago nodule fate map, we have re-analysed four previously characterized mutants with greater accuracy: *nf-ya1-1* (Combier et al., 2006; Laporte et al., 2014), *sickle* (Penmetsa and Cook, 1997), *ipd3* (Horvath et al., 2011; Ovchinnikova et al., 2011; Singh et al., 2014) and *lin-1* (Kuppusamy et al., 2004; Kiss et al., 2009; Guan et al., 2013).

nf-ya1-1
nf-ya1-1 (Combier et al., 2006; Laporte et al., 2014) forms nodules of variable size, but all are markedly smaller than wild-type (wt) nodules. The largest *nf-ya1-1* nodules (Fig. 7B) have about eight cell layers with well-infected cells at their basal part. In these cells, development of rhizobium into nitrogen fixing symbiosomes (supplementary material Fig. S3) is as in wild type, as described by Laporte et al. (2014). These nodules have a

relatively small meristem. In cells derived from it, infection threads are present, but release is blocked. This phenotype suggests that during primordium formation, cell divisions in C4/5 have occurred, and rhizobia are released in these cells. However, the formation of a wild-type-sized meristem that can produce daughter cells competent for bacterial release requires NF-YA1. In addition to these relatively large *nf-ya1-1* nodules, smaller nodules are also formed. These can have only a few layers with fully infected cells (Fig. 7C), the nodule meristem is absent and the nodule is completely surrounded by the nodule endodermis. In these nodules, divisions in C4/5 have most likely occurred to some extent and these cells differentiate into wild-type-like infected cells. However, the formation of a meristem (from C3) appears to be blocked.

To examine these observations in more detail, we studied nodule primordia of the *nf-ya1-1* mutant. Roots were sectioned at 1-5 dpi. This showed that primordia are rather diverse, which is well in line with the diverse nodule phenotypes. The largest primordia are composed of cells derived from pericycle up to C3 (Fig. 8A). Cells derived from C4/5 are infected and contain released bacteria that, in wild type, is a hallmark of stage VI (Fig. 8B); several of these
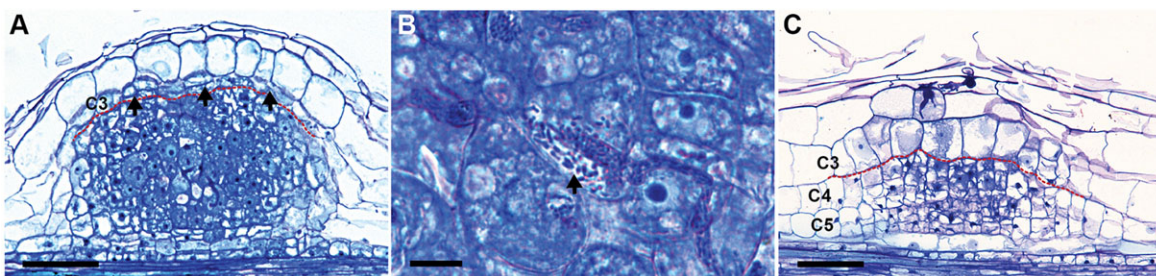

Fig. 8. Reduced cell division in C3 of *nf-ya1-1* nodule primordia. (A) Relatively large *nf-ya1-1* nodule primordium with bacteria release in C4/5-derived cells; the number of C3-derived cells is less than in wild type at stage III or VI (arrows). (B) Bacteria are released from infection threads (arrow) (magnification of the primordium A). (C) A *nf-ya1-1* nodule primordium with about eight cell layers derived from C4/5 and no periclinal division in C3. In A and C, a red line indicates the border between cells derived from C3 and C4. Scale bars: 75 µm in A,C; 10 µm in B.

DEVELOPMENT

infected cells have already enlarged (Fig. 8A). In such primordia, some periclinal divisions have occurred in C3-derived cells, but markedly less than in wild-type stage VI. It seems that such primordia can develop into the relatively large *nf-ya1-1* nodules with a small meristem and hampered bacterial release in its daughter cells. In addition, markedly smaller primordia are formed, where cell divisions have occurred in C4/5, albeit with a lower frequency. Furthermore, only a few anticlinal divisions, no periclinal divisions in C3 and no bacteria release have occurred (Fig. 8C). Such primordia probably develop into the small nodules that lack a meristem.

Using our fate map, we have thus been able not only to confirm and to describe more thoroughly that meristem formation is hampered in the *nf-ya1-1* mutant, but also to show that the well-infected cells inside mutant nodules are derived from C4/5. Furthermore, the cells that are derived from the (small) nodule meristem cells cannot differentiate into cells competent for bacterial release. The latter implies that release of rhizobia in primordia cells derived from C4/5 is not affected in the *nf-ya1-1* mutant, whereas in daughter cells derived from the meristem release requires NF-YA1. Our data also suggest that NF-YA1 is required for proper nodule meristem formation.

sickle

sickle makes markedly more root nodules than wild type as it contains a mutated ethylene signalling gene. The nodule histology of this mutant is in general considered to be wild-type-like (Penmetsa and Cook, 1997). We sectioned about 50 *sickle* nodules that are formed at the 'sickle'-shaped zone (supplementary material Fig. S4A) (Penmetsa and Cook, 1997). The vast majority has about eight (or fewer) layers with well-infected cells. These nodules have no meristem and are surrounded by the endodermis (Fig. 9A). This mutant also forms a few nodules that are morphologically more similar to wild type (Fig. 9B; supplementary material Fig. S4B). However, their size is much smaller than wild type, indicating a sub-optimal functioning meristem (Figs 9C and 4C). So, the defect in ethylene signalling has a positive effect on nodule primordium

formation, but directly or indirectly has a strong negative effect on nodule meristem formation.

sickle was previously used by Timmers et al. (1999) to study the timing of meristem formation and infection thread growth. However, as the sickle mutant is disturbed in nodule meristem formation, these studies might not provide reliable insight into the timing of these processes in wild-type nodules.

ipd3

The fate map studies show that infection threads have passed C3 before periclinal divisions are induced. This suggests that nodule primordia will not be infected when infection thread growth is delayed compared with divisions in C3. IPD3 is a transcriptional regulator that interacts with the kinase CCaMK and is essential for release of bacteria from infection threads (Horvath et al., 2011; Ovchinnikova et al., 2011; Singh et al., 2014). The Medicago *ipd3* (*Mtsym1-1/TE7*) mutant can form nodules with a meristem and numerous infection threads from which rhizobia are not released. However, many nodules remain very small and lack infection threads (Fig. 10A) (Ovchinnikova et al., 2011).

To test whether lack of infection threads in primordia is due to delayed infection thread growth in the outer cortex, serial sections of roots (1-5 dpi) were made. Two types of primordia were detected. One type is similar to wild type (Fig. 10B). C4/5 have formed about eight cell layers and these cells contain infection threads (i.e. the infection threads have successfully passed C3). These primordia probably develop into nodules containing numerous infection threads. The other type of primordium is composed of cells derived from C5, C4 and C3. C3 has already periclinal divided several times, whereas the infection thread has only reached the outer cortex (Fig. 10C). These primordia probably result in small non-infected nodules (Fig. 10A) and this is consistent with the hypothesis that infection threads can no longer traverse C3 when periclinal divisions have been induced (stage IV). In this way, a few hours difference in reaching or passing C3 can result in a major difference in nodule development.
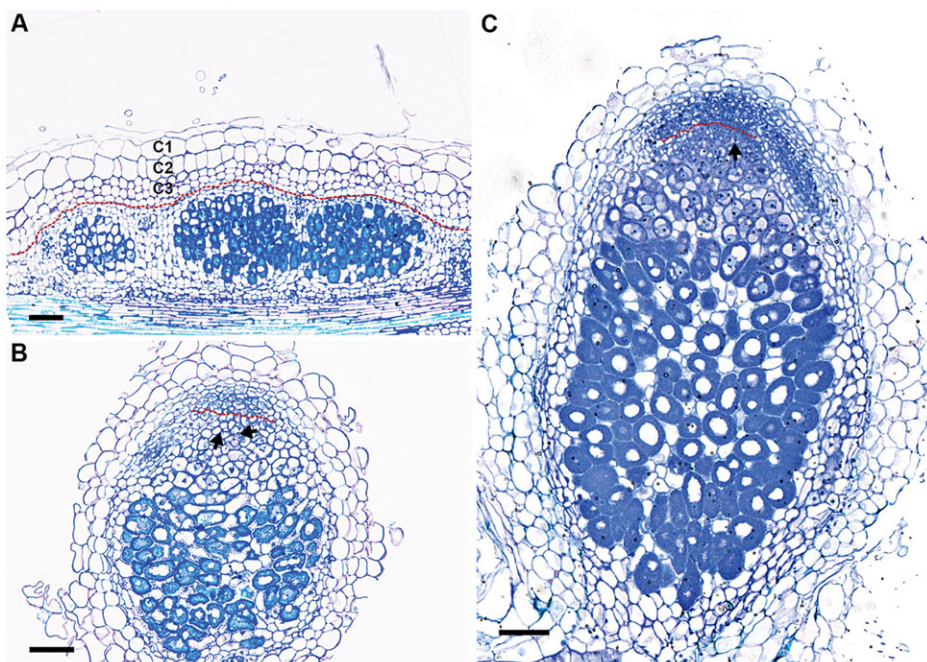

Fig. 9. Meristem formation is hampered in some *sickle* nodules. Two-week-old *sickle* (A,B) and wild-type (C) nodules. (A) *sickle* nodules that are 'fused' have no meristem and are surrounded by an endodermis. (B) A *sickle* nodule is smaller than a (C) wild-type nodule. In A, a red line indicates the border between cells derived from C3 and C4, and from nodule meristem and infection zone in B and C. Infection threads are indicated by arrows (B,C). Scale bars: 75 µm.
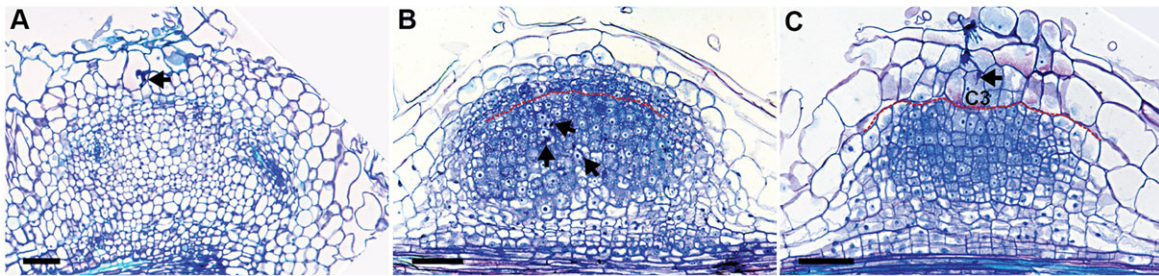
Fig. 10. Infection thread failed to pass the future nodule meristem cells (C3) before stage IV in an *ipd3* mutant. (A) A small non-infected *ipd3* nodule with infection thread (arrow) arrested in outer cortex layers. (B,C) Nodule primordia with infection threads (arrows) successfully reached cells derived from C4/5 (B) and failed to pass through C3 at stage IV (C). In B and C, a red line indicates the border between cells derived from C3 and C4. Scale bars: 75 µm.

lin-1

Rhizobium induced cell division in pericycle and endodermis is arrested at an early stage (II) of development. Some Medicago mutants form nodules with central vascular bundles, whereas wild-type nodules have peripheral vascular bundles. We hypothesize that this is due to more extensive divisions in pericycle and endodermis. An example is *LIN*, which is essential for infection (Kuppusamy et al., 2004; Kiss et al., 2009; Guan et al., 2013) and codes for a E3 ubiquitin ligase. *lin-1* (Kuppusamy et al., 2004) forms non-infected nodules with central vascular bundles (Fig. 11A).

We tested our hypothesis in *lin-1* primordia by using the endodermis marker (*AtCASP1::GUS*). In several primordia, cortical divisions (C4/5) are at stage III-IV, whereas pericycle and endodermis divisions are at stage V or have divided even more frequently (Fig. 11B). In addition to that, C3 divisions are in between stage II-IV and never go further than stage IV. This indicates that the higher mitotic activity of pericycle and endodermis probably leads to the formation of central vascular bundles (Fig. 11C). The phenotype of the *lin-1* mutant suggests that the expression of this gene is important to block cell divisions in endodermis/pericycle-derived cells at an early stage of development.

Integrated model for cell fate control and initiation of cell division

In this study, we produced a fate map for Medicago root nodules. This fate map is summarized in the cartoon shown in Fig. 12 and Table 1. In a mature nodule, about eight cell layers of the basal part of the nodule tissue are derived directly from the nodule primordium (C4/5 derived) and not from the meristem. The uninfected basal tissues develop from primordium cells, which are derived from endodermis and pericycle. The nodule meristem is derived from a single central cortical layer (C3) and when the meristem becomes functional at stage VI, it continuously adds cells to the different nodule tissues.

Nodule primordium formation starts with cell divisions in the pericycle and subsequently extends towards more outer layers. When pericycle cells are mitotically activated by Nod factors secreted by rhizobia, the bacteria are still present at or in the epidermis. As Nod factors are rather immobile signal molecules (Goedhart et al., 2000), perception of Nod factors at the epidermis most likely triggers mitotic activity in inner root cell layers. So how could an exogenously applied signal lead to cell division starting in the cell layer that is most remote, while the cells closest to the signal respond last?

Previously, we made a theoretical model to investigate how Nod factors can induce cortical cell divisions (Deinum et al., 2012). It is known that Nod factor perception leads to cytokinin signalling (Op den Camp et al., 2011), whereas cortical cell division is associated with increased auxin (Mathesius et al., 1998). Cytokinin is known to affect negatively the accumulation of auxin efflux carriers (PIN) in the plasma membrane (Dello Ioio et al., 2008; Marhavy et al., 2011). Therefore, we postulated that Nod factor signalling induces the decrease of the level of PIN protein in all cortical cell layers of the region responding to Nod factors. This block of cortical cells was named the 'controlled area'. This resulted, according to our model, in a local increase of auxin in the cortex that coincided with the site where cortical cell divisions are induced. Here, we include the pericycle and endodermis in the 'controlled area' (Fig. 13A) and focus on the early dynamics of the predicted auxin accumulation in the cell layers where cell division is induced (see supplementary Material and Methods).

For our current simulations, we start from a PIN layout that gives rise to auxin accumulation in inner root layers (Fig. 13B), as
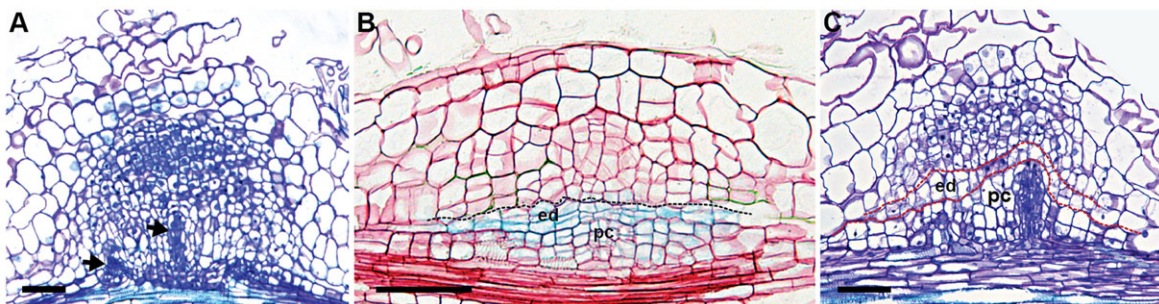

Fig. 11. Extensive cell divisions in root pericycle and endodermis during *lin1-1* nodule primordium development correlates with formation of central vascular bundle. A two-week-old *lin1-1* nodule (A), which has a few central vascular bundles (arrows) and does not have a meristem. (B) In *AtCASP1::GUS*-expressing *lin1-1* roots, a nodule primordium has more endodermis and pericycle divisions than the wild-type stage V primordium. The numbers of C3- and C4/5-derived cells are less or comparable with wild-type cell numbers at stage IV. (C) Central vascular bundles of *lin1-1* nodules are derived from the pericycle. In B and C, the lines confine cells derived from the endodermis. Scale bars: 75 µm.
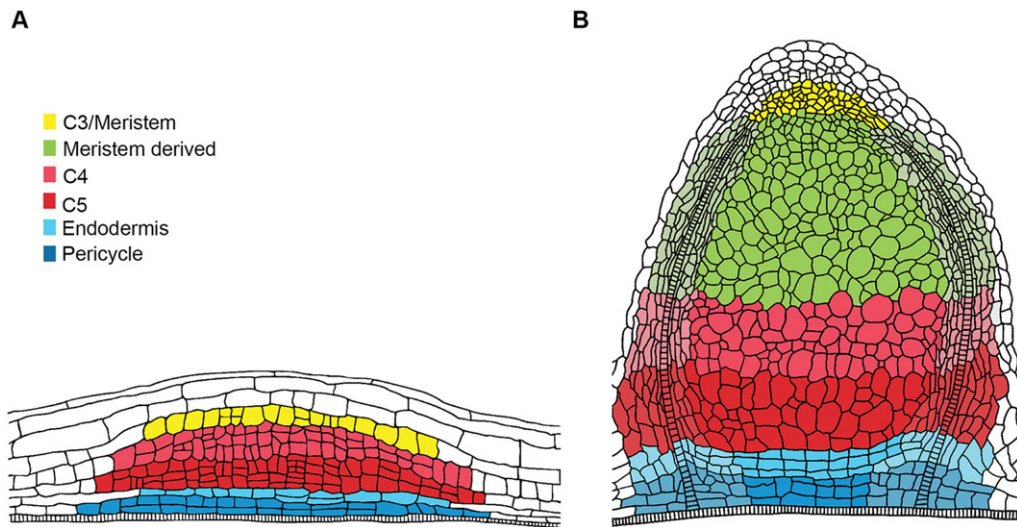
Fig. 12. Indeterminate root nodule fate map, nodule primordium and nodule. (A,B) The origins of cells in primordium (A) and nodule (B) are indicated by the same colour. The origin of the nodule cortex is not shown.

divisions have been observed to coincide with an auxin maximum (Mathesius et al., 1998; T.T.X., unpublished). This layout, and all variants that we have used, produce a root-ward auxin flux in the stele/vascular tissue, and a shoot-ward and inward flux in the cortex.

The reduction of membrane PINs resulted in an increase of the auxin concentration in all cell layers. However, only in the pericycle, endodermis and inner cortical layers did the auxin concentration in the controlled area reach a level similar to or higher than the vascular starting level. Furthermore, in the outer layers, the absolute increase was very small compared with this (Fig. 13C-F;

supplementary material Movie 1). A detailed modelling study of the auxin-sensing system of TIR1-SCF controlled ubiquitylation of Aux/IAA proteins showed it has the potential to detect changes in auxin concentration (Middleton et al., 2010). We therefore plotted the concentration increase in each layer normalized by the concentrations at the beginning and the end of the simulation (Fig. 13G), and the time derivative of these curves (Fig. 13H). This shows that the auxin concentration increased first and fastest in the pericycle, followed by the endodermis and C5, and then by other layers in an outward fashion. The time derivatives (Fig. 13H) clearly show that the pericycle was also the first layer where the increase of

Table 1. Characteristics of the Medicago nodule primordia developmental stages

| Stage	Primordia characteristics	Infection thread tip
I	1. Pericycle: anticlinal divisions	NA
II	1. C4/5: anticlinal divisions	NA
III	1. C3: anticlinal divisions	C3 or C4
	2. C4/5: first periclinal division	
	3. Endodermis: anticlinal divisions	
IV	1. C2: anticlinal divisions	C4/5
	2. C3: first periclinal divisions	
	3. C4/5: cell division continued	
	4. Endodermis/pericycle: first periclinal divisions	
V	1. C3: multi layered (future) meristem	Central part of C4/5-derived cells
	2. C4/5:	
	i. central part cell division stops	
	ii. six to eight cell layers	
	iii. central cells start to enlarge	
	iv. peripheral cells start to differentiate into vascular bundles and peripheral tissues	
	3. Endodermis/pericycle:	
	i. central part cell division stops	
	ii. six to eight cell layers	
	iii. peripheral cells start to differentiate into vascular bundles and peripheral tissues	
VI	1. C3: functional meristem start adding cells to the nodule	Central part of C4/5-derived cells (bacteria released)
	2. C4/5:	
	i. central cells enlarged	
	ii. peripheral cells differentiated into vascular bundles and peripheral tissues	
	3. Endodermis/pericycle:	
	i. central cells differentiated to parenchyma and an endodermis layer with casparian strips	
	ii. peripheral cells differentiated to vascular bundles and peripheral tissues	

NA, not applicable.
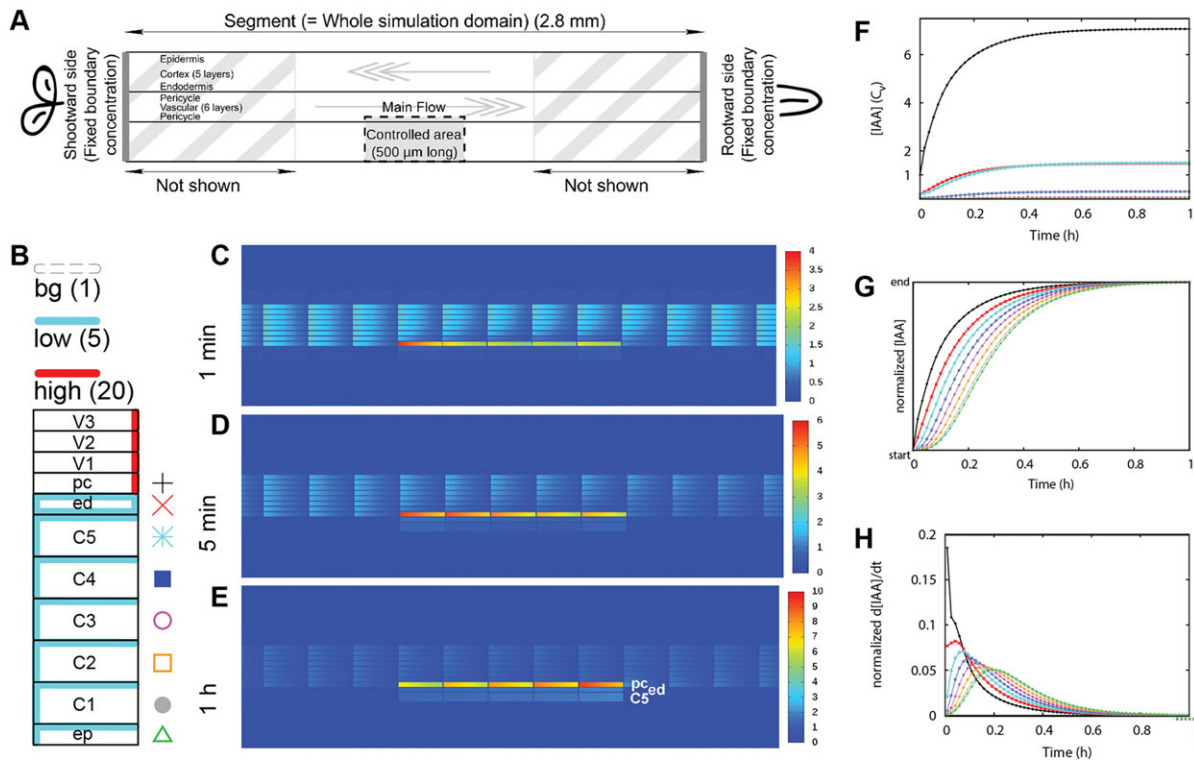
Fig. 13. Auxin accumulation following a local reduction of the effective efflux permeability starts from the inner root layers. (A) Simulations are based on a root segment representing the susceptible zone of Medicago roots (Deinum et. al., 2012). At T=0 s, the efflux is reduced in a block of cells that is five cells long and comprises all cell files from epidermis to pericycle. This we refer to as the 'controlled area'. The PIN distribution (B) of this root segment is such that the main auxin flux in the vascular tissue is rootward and reversed in the cortex. The starting concentration of PINs in each membrane segment is one of three levels: 'high' (red, P_{eff}=20 µm s^{-1}), 'low' (cyan, P_{eff}=5 µm s^{-1}) or 'bg' (background level; white, P_{eff}=1 µm s^{-1}) (Laskowski et al., 2008; Deinum et al., 2012). The colours of the symbols serve as a key for F-H. (C-E) Concentration heat maps of the middle part of the root segment including the controlled area at T=1 min (C), T=5 min (D) and T=1 h (E) (supplementary material Movie 1). (F) The concentration in the middle row of cells is tracked for all cell files in the controlled area. The concentration in the pericycle remains highest, followed by endodermis and inner cortex (C5). (G) When rescaling the concentration in each file from its starting level to the level reached at the end of the simulation (T=1 h), it becomes clear that the concentration in the pericycle increased first, followed by the other layers in an interior to exterior order. The moment of fastest concentration increase, the peaks of the curves in H (time derivative of G, expressed in rescaled concentration units per minute), show the same relative order: starting from the pericycle, 1st vasculature cell layer (V1), 2nd vasculature cell layer (V2) and 3rd vasculature cell layer (V3).

concentration started slowing down; the peaks of these curves occurred in an interior-to-exterior order. Two sets of control simulations – slowing down the dynamics by decreasing all influx and efflux parameters (supplementary material Fig. S5), and changing the cortical auxin distribution of the segment by varying the inward:outward ratio of the cortical PINs (supplementary material Fig. S6) – show that auxin accumulation from the inner layers is a robust feature of the model.

If we use auxin as a proxy for the induction of cell divisions, these results predict that the divisions would start from the interior layers and proceed outwards. This would happen when divisions are controlled both by absolute auxin concentration and the change in auxin concentration. So this model can explain the initial steps (stage I and II) of nodule primordium formation, although it does not address the later stages.

Divisions in pericycle and endodermis are arrested when a few layers are formed. In the *lin* mutant, the arrest of division in these cell layers is delayed and this is correlated with the formation of vasculature in the central region of the nodules. As this vasculature is not well integrated into nodule tissue derived from cortical cells, it underlines the importance of an early block of division in pericycle and endodermis.

In nodule primordia where rhizobia are not released, central tissue cells (and their nuclei) remain small, as in *ipd3* and *lin*. Therefore, it

is probable that induction of endoreduplication requires release of rhizobia from infection threads or vice versa.

Our nodule fate map underlines the impact of the multistep nature of nodule formation, as well as the involvement of different root tissues in nodule formation. Similar processes can occur at different time points and in different cell types. A clear example is the release of rhizobia from infection threads in nodule primordium cells and in daughter cells of the meristem. In the latter case, NF-YA1 appeared to be essential for release, whereas release is not affected in primordium cells of the *nf-ya1-1* mutant. This shows that similar processes can be controlled by different mechanisms (or with different stringency) during subsequent steps of nodule development. In conclusion, we have shown that a nodule fate map is indispensable for identification of the affected developmental steps in nodulation mutants.

MATERIALS AND METHODS
Plant material, bacterial strains and constructs
M. truncatula accession Jemalong A17 plants were used to study nodule primordium formation. This accession is also used to generate *Agrobacterium rhizogenes* (strain MSU440)-mediated transgenic roots, as previously described (Limpens et al., 2004). Construct details are in the supplementary Material and Methods. Another *M. truncatula* accession used is R108. This accession has roots with five or four cortical layers. In both root types, nodule meristem is derived from C3. In roots with five cortical cell layers, the formation of primordia is similar to that described for A17 in Fig. 1.

M. truncatula accession R108 seedlings were used to make the stable *AtCyclB1.1::GUS* (Burssens et al., 2000) transgenic line by using *Agrobacterium tumefaciens* (strain AGL1) and following an established protocol (Chabaud et al., 2003). *MtCCS52A::GUS* is also introduced in R108 (Vinardell et al., 2003). The symbiotic mutants re-analysed in this study have been described previously: *nf-ya1-1* (Laporte et al., 2014), *sickle* (Penmetsa and Cook, 1997), *ipd3* (Ovchinnikova et al., 2011) and *lin1-1* (Kuppusamy et al., 2004). The surface sterilization and germination of Medicago seeds were performed as previously described (Limpens et al., 2004). Roots of A17 were inoculated with *Sinorhizobium meliloti* (*S. meliloti*) strain 2011 and roots of R108 were inoculated with *S. meliloti* Rm41.

Histochemical β-glucuronidase (GUS) staining

Transgenic plant material (nodules and part of roots) containing GUS constructs were incubated in GUS buffer [3% sucrose, 2 mM $K_3Fe(CN)_6$, 2 mM $K_4Fe(CN)_6$, 10 mM EDTA and 1 mg/ml X-Gluc salt in 100 mM phosphate buffer solution (pH 7.0)] under vacuum for 30 min and then at 37°C for 3-24 h (Jefferson et al., 1987).

Tissue embedding, sectioning and section staining

Root segments and nodules were fixed at 4°C overnight with 4% paraformaldehyde (w/v), 5% glutaraldehyde (v/v) in 0.05 M nitrate phosphate buffer (pH 7.2). The fixed material was dehydrated in an ethanol series and subsequently embedded in Technovit 7100 (Heraeus Kulzer) according to the manufacturer's protocol. Longitudinal sections (5 μm) were made by using a RJ2035 microtome (Leica Microsystems, Rijswijk, The Netherland) stained for 5 min in 0.05% Toluidine Blue O. For GUS-stained plant material, 9-10 μm longitudinal sections were stained for 15 min in 0.1% Ruthenium Red. Sections were analysed by using a DM5500B microscope equipped with a DFC425C camera (Leica Microsystems, Wetzlar, Germany).

Simulation methods

We used our previously described simulation platform (Deinum et al., 2012), for details, see supplementary Material and Methods.

References

Bond, L. (1948). Origin and developmental morphology of root nodules of *Pisum Sativum*. *Bot. Gaz.* **109**, 411-434.

Brewin, N. J. (1991). Development of the legume root nodule. *Annu. Rev. Cell Biol.* **7**, 191-226.

Brewin, N. J. (2004). Plant cell wall remodelling in the rhizobium-legume symbiosis. *Crit. Rev. Plant Sci.* **23**, 293-316.

Burssens, S., Himanen, K., van de Cotte, B., Beeckman, T., Van Montagu, M., Inzé, D. and Verbruggen, N. (2000). Expression of cell cycle regulatory genes and morphological alterations in response to salt stress in *Arabidopsis thaliana*. *Planta* **211**, 632-640.

Chabaud, M., de Carvalho-Niebel, F. and Barker, D. G. (2003). Efficient transformation of *Medicago truncatula* cv. Jemalong using the hypervirulent *Agrobacterium tumefaciens* strain AGL1. *Plant Cell Rep.* **22**, 46-51.

Combier, J.-P., Frugier, F., de Billy, F., Boualem, A., El-Yahyaoui, F., Moreau, S., Vernie, T., Ott, T., Gamas, P. and Crespi, M. et al. (2006). MtHAP2-1 is a key transcriptional regulator of symbiotic nodule development regulated by microRNA169 in *Medicago truncatula*. *Genes Dev.* **20**, 3084-3088.

Deinum, E. E., Geurts, R., Bisseling, T. and Mulder, B. M. (2012). Modeling a cortical auxin maximum for nodulation: different signatures of potential strategies. *Front. Plant Sci.* **3**, 96.

Dello Ioio, R., Nakamura, K., Moubayidin, L., Perilli, S., Taniguchi, M., Morita, M. T., Aoyama, T., Costantino, P. and Sabatini, S. (2008). A genetic framework for the control of cell division and differentiation in the root meristem. *Science* **322**, 1380-1384.

Di Laurenzio, L., Wysocka-Diller, J., Malamy, J. E., Pysh, L., Helariutta, Y., Freshour, G., Hahn, M. G., Feldmann, K. A. and Benfey, P. N. (1996). The SCARECROW gene regulates an asymmetric cell division that is essential for generating the radial organization of the Arabidopsis root. *Cell* **86**, 423-433.

Dudley, M. E., Jacobs, T. W. and Long, S. R. (1987). Microscopic studies of cell divisions induced in alfalfa roots by *Rhizobium meliloti*. *Planta* **171**, 289-301.

Goedhart, J., Hink, M. A., Visser, A. J. W. G., Bisseling, T. and Gadella, T. W. J.,Jr. (2000). *In vivo* fluorescence correlation microscopy (FCM) reveals accumulation and immobilization of Nod factors in root hair cell walls. *Plant J.* **21**, 109-119.

Guan, D., Stacey, N., Liu, C., Wen, J., Mysore, K. S., Torres-Jerez, I., Vernié, T., Tadege, M., Zhou, C. and Wang, Z.-Y. et al. (2013). Rhizobial infection is associated with the development of peripheral vasculature in nodules of *Medicago truncatula*. *Plant Physiol.* **162**, 107-115.

Hadri, A. E., Spaink, H. P., Bisseling, T. and Brewin, N. J. (1998). Diversity of root nodulation and rhizobial infection processes. In *The Rhizobiaceae*: *Molecular Biology of Model Plant Associated Bacteria* (ed. H. P. Spaink, A. Kondorosi, and P. Hooykaas,), pp. 347-360. The Netherlands: Springer.

Herrbach, V., Rembliére, C., Gough, C. and Bensmihen, S. (2014). Lateral root formation and patterning in *Medicago truncatula*. *J. Plant Physiol.* **171**, 301-310.

Horváth, B., Yeun, L. H., Domonkos, A., Halász, G., Gobbato, E., Ayaydin, F., Miró, K., Hirsch, S., Sun, J. H. and Tadege, M. et al. (2011). *Medicago truncatula* IPD3 is a member of the common symbiotic signaling pathway required for rhizobial and mycorrhizal symbioses. *Mol. Plant Microbe Interact.* **24**, 1345-1358.

Ivanov, S., Fedorova, E. E., Limpens, E., De Mita, S., Genre, A., Bonfante, P. and Bisseling, T. (2012). *Rhizobium*-legume symbiosis shares an exocytotic pathway required for arbuscule formation. *Proc. Natl. Acad. Sci. USA* **109**, 8316-8321.

Jefferson, R. A., Kavanagh, T. A. and Bevan, M. W. (1987). Gus fusions: β-glucuronidase as a sensitive and versatile gene fusion marker in higher-plants. *EMBO J.* **6**, 3901-3907.

Kiss, E., Olah, B., Kalo, P., Morales, M., Heckmann, A. B., Borbola, A., Lozsa, A., Kontar, K., Middleton, P. and Downie, J. A. et al. (2009). LIN, a novel type of U-Box/WD40 protein, controls early infection by rhizobia in legumes. *Plant Physiol.* **151**, 1239-1249.

Kuppusamy, K. T., Endre, G., Prabhu, R., Penmetsa, R. V., Veereshlingam, H., Cook, D. R., Dickstein, R. and Van den Bosch, K. A. (2004). LIN, a *Medicago truncatula* gene required for nodule differentiation and persistence of rhizobial infections. *Plant Physiol.* **136**, 3682-3691.

Lancelle, S. A. and Torrey, J. G. (1985). Early development of *Rhizobium*-induced root nodules of *Parasponia rigida*. II. Nodule morphogenesis and symbiotic development. *Can. J. Bot.* **63**, 25-35.

Laporte, P., Lepage, A., Fournier, J., Catrice, O., Moreau, S., Jardinaud, M.-F., Mun, J.-H., Larrainzar, E., Cook, D. R. and Gamas, P. et al. (2014). The CCAAT box-binding transcription factor NF-YA1 controls rhizobial infection. *J. Exp. Bot.* **65**, 481-494.

Laskowski, M., Grieneisen, V. A., Hofhuis, H., Hove, C. A. T., Hogeweg, P., Marée, A. F. M. and Scheres, B. (2008). Root system architecture from coupling cell shape to auxin transport. *PLoS Biol.* **6**, 2721-2735.

Lefebvre, B., Timmers, T., Mbengue, M., Moreau, S., Herve, C., Toth, K., Bittencourt-Silvestre, J., Klaus, D., Deslandes, L. and Godiard, L. et al. (2010). A remorin protein interacts with symbiotic receptors and regulates bacterial infection. *Proc. Natl. Acad. Sci. USA* **107**, 2343-2348.

Lerouge, P., Roche, P., Faucher, C., Maillet, F., Truchet, G., Promé, J. C. and Dénarié, J. (1990). Symbiotic host-specificity of *Rhizobium meliloti* is determined by a sulphated and acylated glucosamine oligosaccharide signal. *Nature* **344**, 781-784.

Libbenga, K. R. and Harkes, P. A. A. (1973). Initial proliferation of cortical cells in the formation of root nodules in *Pisum sativum* L. *Planta* **114**, 17-28.

Limpens, E., Ramos, J., Franken, C., Raz, V., Compaan, B., Franssen, H., Bisseling, T. and Geurts, R. (2004). RNA interference in *Agrobacterium rhizogenes*-transformed roots of *Arabidopsis* and *Medicago truncatula*. *J. Exp. Bot.* **55**, 983-992.

Marhavý, P., Bielach, A., Abas, L., Abuzeineh, A., Duclercq, J., Tanaka, H., Parezova, M., Petrášek, J., Friml, J. and Kleine-Vehn, J. et al. (2011). Cytokinin modulates endocytic trafficking of PIN1 auxin efflux carrier to control plant organogenesis. *Dev. Cell* **21**, 796-804.

Mathesius, U., Bayliss, C., Weinman, J. J., Schlaman, H. R. M., Spaink, H. P., Rolfe, B. G., McCully, M. E. and Djordjevic, M. A. (1998). Flavonoids synthesized in cortical cells during nodule initiation are early developmental markers in white clover. *Mol. Plant Microbe Interact.* **11**, 1223-1232.

DEVELOPMENT

Middleton, A. M., King, J. R., Bennett, M. J. and Owen, M. R. (2010). Mathematical modelling of the Aux/IAA negative feedback loop. *Bull. Math. Biol.* **72**, 1383-1407.

Nap, J.-P. and Bisseling, T. (1990). Developmental biology of a plant-prokaryote symbiosis: the legume root nodule. *Science* **250**, 948-954.

Nutman, P. S. (1948). Physiological studies on nodule formation.1. The relation between nodulation and lateral root formation in red clover. *Ann. Bot.* **12**, 81-96.

Op den Camp, R. H. M., De Mita, S., Lillo, A., Cao, Q., Limpens, E., Bisseling, T. and Geurts, R. (2011). A phylogenetic strategy based on a legume-specific whole genome duplication yields symbiotic cytokinin type-A response regulators. *Plant Physiol.* **157**, 2013-2022.

Ovchinnikova, E., Journet, E.-P., Chabaud, M., Cosson, V., Ratet, P., Duc, G., Fedorova, E., Liu, W., Op den Camp, R. and Zhukov, V. et al. (2011). IPD3 controls the formation of nitrogen-fixing symbiosomes in pea and *Medicago spp*. *Mol. Plant Microbe Interact.* **24**, 1333-1344.

Penmetsa, R. V. and Cook, D. R. (1997). A legume ethylene-insensitive mutant hyperinfected by its rhizobial symbiont. *Science* **275**, 527-530.

Roppolo, D., De Rybel, B., Tendon, V. D., Pfister, A., Alassimone, J., Vermeer, J. E. M., Yamazaki, M., Stierhof, Y.-D., Beeckman, T. and Geldner, N. (2011). A novel protein family mediates Casparian strip formation in the endodermis. *Nature* **473**, 380-383.

Roth, L. E. and Stacey, G. (1989). Bacterium release into host cells of nitrogen-fixing soybean nodules the symbiosome membrane comes from three sources. *Eur. J. Cell Biol.* **49**, 13-23.

Singh, S., Katzer, K., Lambert, J., Cerri, M. and Parniske, M. (2014). CYCLOPS, a DNA-binding transcriptional activator, orchestrates symbiotic root nodule development. *Cell Host Microbe* **15**, 139-152.

Sugimoto, K., Gordon, S. P. and Meyerowitz, E. M. (2011). Regeneration in plants and animals: dedifferentiation, transdifferentiation, or just differentiation? *Trends Cell Biol*. **21**, 212-218.

Timmers, A. C. J., Auriac, M. C. and Truchet, G. (1999). Refined analysis of early symbiotic steps of the Rhizobium-Medicago interaction in relationship with microtubular cytoskeleton rearrangements. *Development* **126**, 3617-3628.

Van de Wiel, C., Norris, J. H., Bochenek, B., Dickstein, R., Bisseling, T. and Hirsch, A. M. (1990). Nodulin gene-expression and Enod2 localization in effective, nitrogen-fixing and ineffective, bacteria-free nodules of alfalfa. *Plant Cell* **2**, 1009-1017.

Vermeer, J. E. M., von Wangenheim, D., Barberon, M., Lee, Y., Stelzer, E. H. K., Maizel, A. and Geldner, N. (2014). A spatial accommodation by neighboring cells is required for organ initiation in *Arabidopsis*. *Science* **343**, 178-183.

Vinardell, J. M., Fedorova, E., Cebolla, A., Kevei, Z., Horvath, G., Kelemen, Z., Tarayre, S., Roudier, F., Mergaert, P. and Kondorosi, A. et al. (2003). Endoreduplication mediated by the anaphase-promoting complex activator CCS52A is required for symbiotic cell differentiation in Medicago truncatula nodules. *Plant Cell* **15**, 2093-2105.

Yang, W. C., Deblank, C., Meskiene, I., Hirt, H., Bakker, J., Vankammen, A., Franssen, H. and Bisseling, T. (1994). Rhizobium Nod factors reactivate the cell-cycle during infection and nodule primordium formation, but the cycle is only completed in primordium formation. *Plant Cell* **6**, 1415-1426.

DEVELOPMENT

Material and Methods

Simulation methods

We used our previously described simulation platform (Deinum et al., 2012) to simulate changes in auxin transport in root segments representing the susceptible zone of legume roots. Inside cells and within the apoplast, auxin moves by diffusion with diffusion constants 300 μm^2 s^{-1} and 44 μm^2 s^{-1}, respectively. Auxin transport over membranes is modeled using effective permeabilities. This results in an outward flux of $J_{mem} = C_{cell} P_{eff} - C_{wall} P_{inf}$, with negative values indicating a net inward flux. In this, C_{cell} and C_{wall} are the concentrations in the pixels on either side of the membrane, P_{eff} is the local effective efflux permeability, which starts at one of three levels ("high" = 20 μm s^{-1}, "low" = 5 μm s^{-1}, or "bg" (background level) = 1 μm s^{-1} as shown in fig. 3B), and P_{inf} = 20 μm s^{-1} the effective influx permeability, as shown in figure 13A.

The PIN layout of these root segments is derived from the model of (Laskowski et al., 2008), which is based on their experimental observations in Arabidopsis, with cell sizes and number of cortical layers adapted to the Medicago geometry. Individual cells are 100 μm long and 20 μm (cortex) or 10 μm (all others) wide.

In the middle of the segment we have indicated a five cell long block of cells, comprising epidermis to pericycle on one side of the root, which we call the "controlled area". At T = 0 we reduce all P_{eff} parameters in the controlled area by a factor 10. Using larger factors did not affect the qualitative behaviour of the model, i.e., any of the effects described in the main text. It only resulted in larger absolute increases of the auxin concentration and corresponding increases of the time to reach the new steady state concentration (not shown).

The full segments are 28 cells long to avoid boundary effects near the controlled area. For further details and references, see (Deinum et al., 2012). Because we focus on early events we used a smaller integration time step of 0.1 second.

Deinum, E. E., Geurts, R., Bisseling, T. and Mulder, B. M. (2012). Modeling a cortical auxin maximum for nodulation: different signatures of potential strategies. *Front Plant Sci.* **3**, 96.
Laskowski, M., Grieneisen, V. A., Hofhuis, H., Hove, C. A. t., Hogeweg, P., Maree, A. F. M. and Scheres, B. (2008). Root system architecture from coupling cell shape to auxin transport. *PLoS Biology* **6**, 2721-2735.

Constructs

The *AtCASP1::GUS* construct is described in Roppolo et al., 2011. For *MtENOD40::GUS* and *AtSCR::GUS* constructs, DNA fragments of putative promoters were amplified from *M. truncatula* and *A. thaliana* genomic DNA respectively using primer combinations listed in Table S1 and **Phusion™ High-Fidelity DNA Polymerase** (Finnzymes).Then, the Gateway® technology (Invitrogen) was used to create genetic promoter-GUS constructs (Karimi et al., 2002). For *MtENOD40::GUS*, the pENTR™/D-TOPO® Cloning Kits (Invitrogen) was used to create entry clones. The entry vector was recombined into Gateway®-compatible binary vector pKGW-RR, that contains GUS reporter gene and *AtUBQ10::DsRED1* as a selection marker (Limpens et al., 2004), by using Gateway® LR Clonase® II enzyme mix (Invitrogen). For *AtSCR::GUS*, the *AtSCR* DNA fragment was introduced into Gateway® donor vector pENTR4-1, GUS reporter gene into pENTR1-2 and 35S CaMV terminator into pENTR2-3, using Gateway® BP Clonase® II enzyme mix. These entry vectors were recombined into Gateway®-compatible binary vector pKGW-RR-MGW, that contains *AtUBQ10::DsRED1* as a selection marker using Gateway® LR Clonase® II Plus enzyme mix (Invitrogen).

Karimi, M., Inze, D. and Depicker, A. (2002). GATEWAY^{TM} vectors for *Agrobacterium*-mediated plant transformation. *Trends Plant Sci.* **7**, 193-195.

Limpens, E., Ramos, J., Franken, C., Raz, V., Compaan, B., Franssen, H., Bisseling, T. and Geurts, R. (2004). RNA interference in *Agrobacterium rhizogenes*-transformed roots of *Arabidopsis* and *Medicago truncatula*. *J. Exp. Bot.* **55**, 983-992.

Roppolo, D., De Rybel, B., Tendon, V. D., Pfister, A., Alassimone, J., Vermeer, J. E., Yamazaki, M., Stierhof, Y. D., Beeckman, T. and Geldner, N. (2011). A novel protein family mediates Casparian strip formation in the endodermis. *Nature* **473**, 380-383.
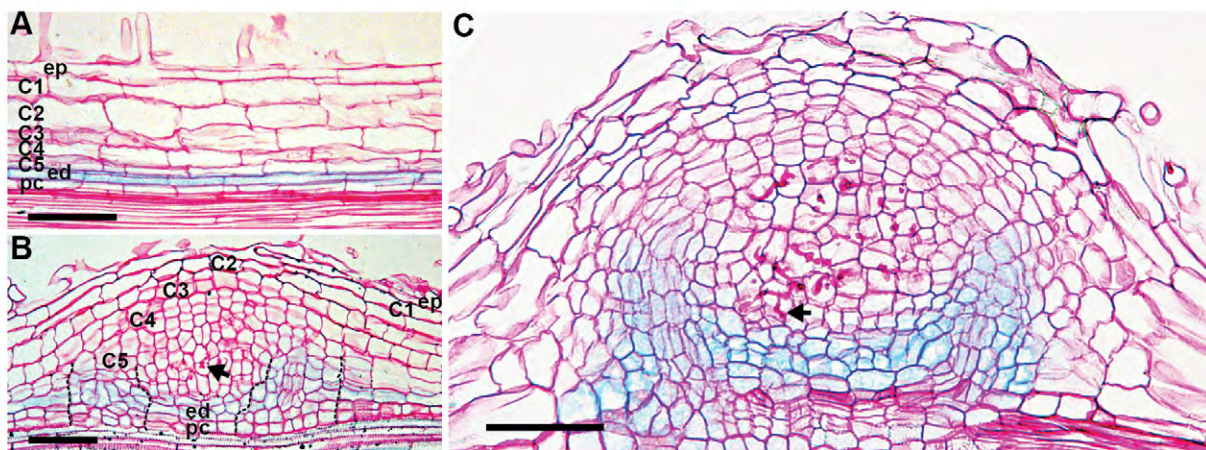
Fig. S1. *AtSCR::GUS* is expressed in endodermis (A) and cells derived from endodermis (B) and these cells are not infected by rhizobium (B-C) (Infection threads are indicated by arrows).

In B, cells at the periphery region (indicated in between black lines) will differentiate into nodule parenchyma include vascular bundles and endodermis.
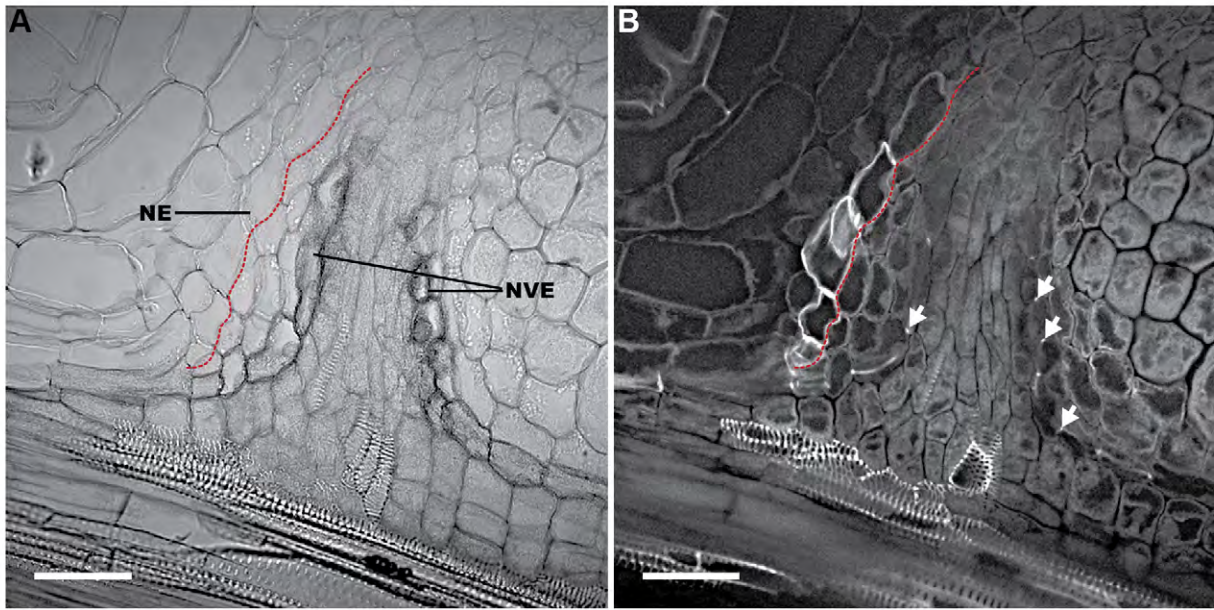
Bars, 75 μm.

Fig. S2. Casparian strips are present in cells where *AtCASP1::GUS* is expressed.

Split channels of Fig. 5D. (A) *AtCASP1::GUS* is expressed in NVE but not in NE; (B) Casparian strips (arrows) are present in NVE but not in NE.
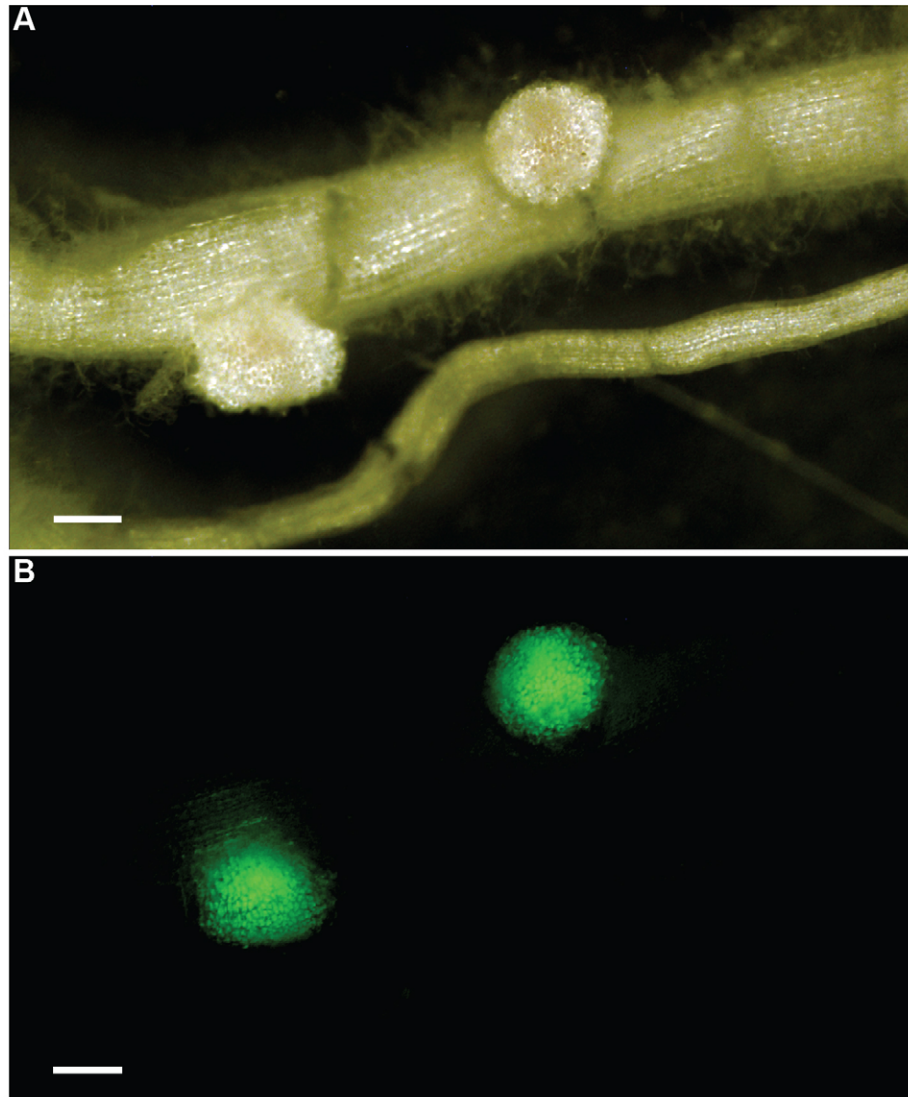
Bars, 50 μm.

Fig. S3. *Sinorhizobium meliloti* strain 2011 expresses nifH::GFP in *nf-ya1-1* nodules.
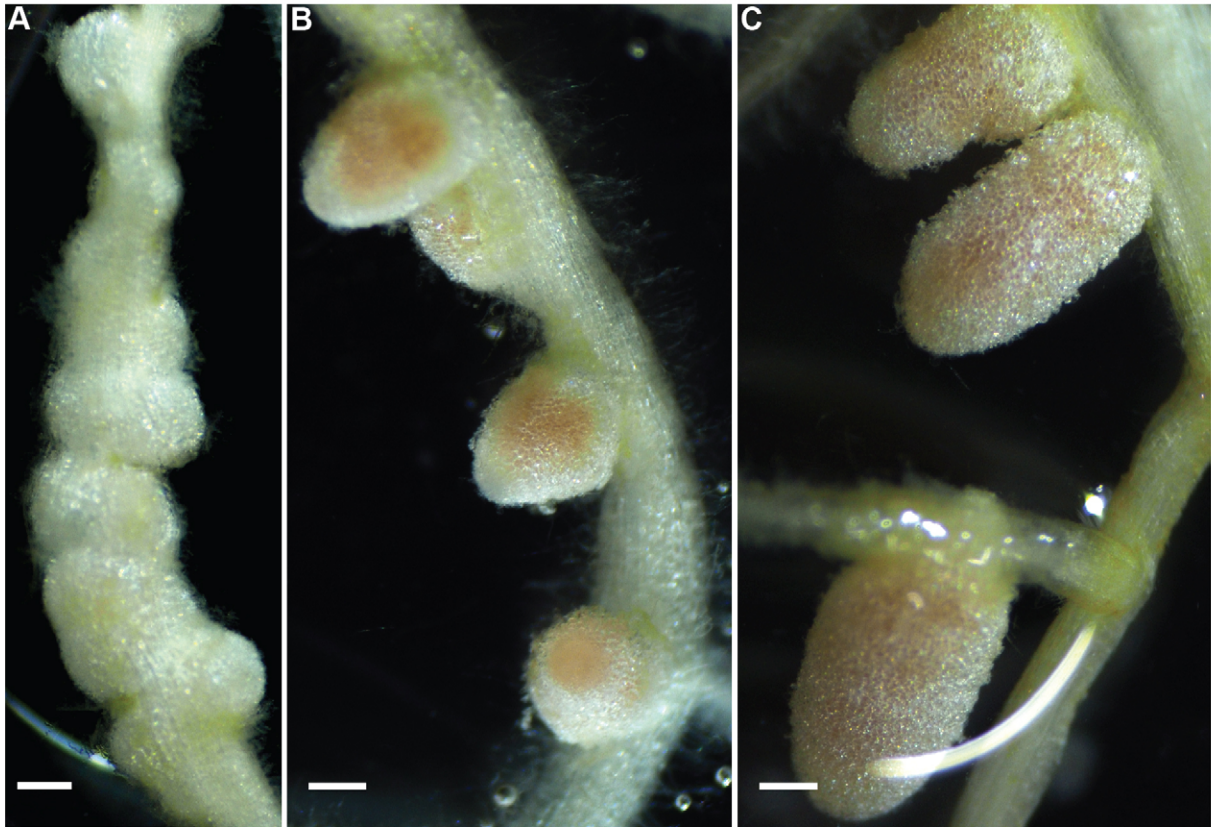
Bars, 250 μm.

Fig. S4. Three weeks old *sickle* nodules (A-B) in comparison to wt nodules (C)

(A) Nodules formed at the "sickle" shaped zone. (B) Small pink nodules.
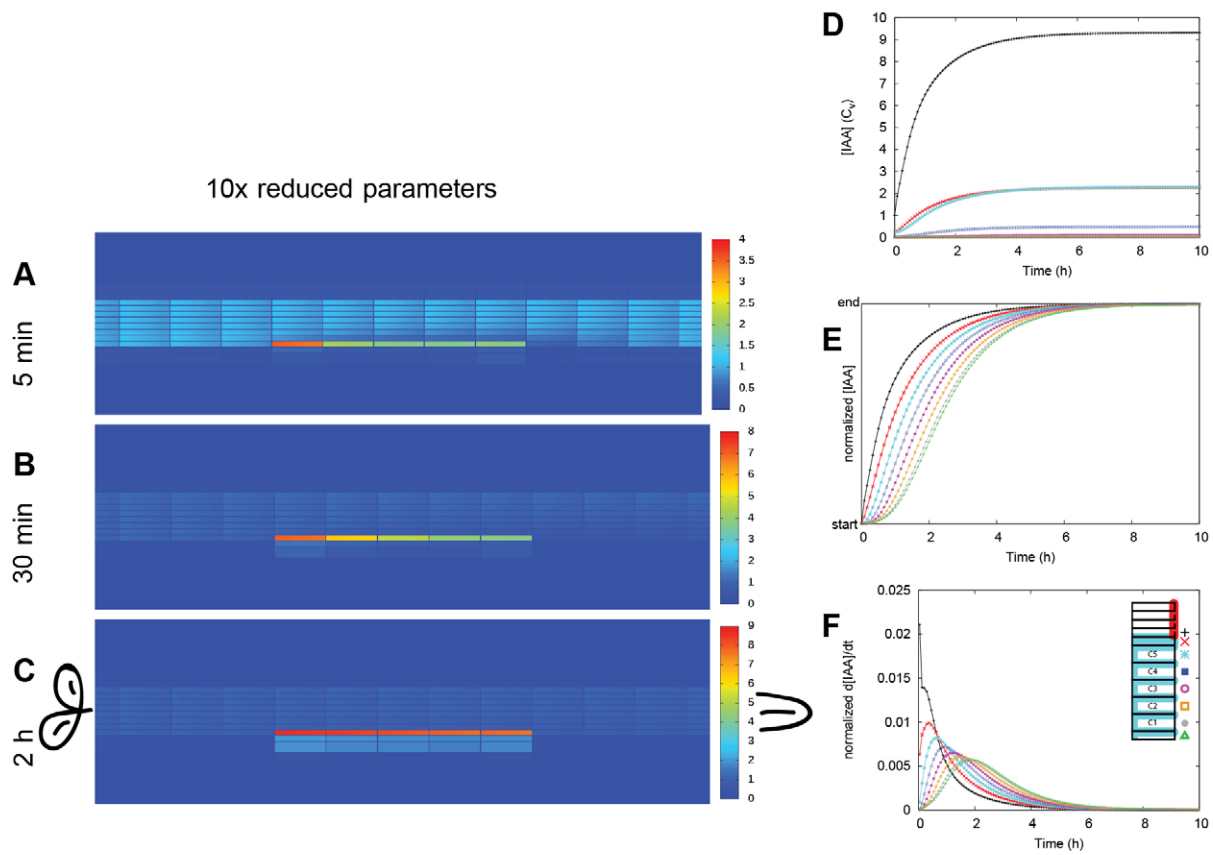
Bars, 250 μm.

Fig. S5. Also with slowed down auxin dynamics, auxin accumulation following a local 10x reduction of the effective efflux permeability starts from the inner root layers.

The starting concentration of PINs in each membrane segment is one of three levels: "high" (red, P_{eff} =2 µm s^{-1}), "low" (cyan, P_{eff} =0.5 µm s^{-1}), or "bg" (white, P_{eff} =0.1 µm s^{-1}) (Deinum et. al, 2012). (A-C) Concentration heat maps of the part of the root segment including the controlled area at T=5 min (A), T=30 min (B) and T=2 h (C). (D) The concentration in the middle row of cells is tracked for all cell files in the controlled area. The concentration in the pericycle remains highest, followed by endodermis and inner cortex (C5). (E) When rescaling the concentration in each file from its starting level to the level reached at the end of the simulation (T=20 h), it becomes clear that the concentration in the pericycle increased first, followed by the other layers in an interior to exterior order. The moment of fastest concentration increase, the peaks of the curves in F (time derivative of E, expressed in rescaled concentration units per minute), showed the same relative order.
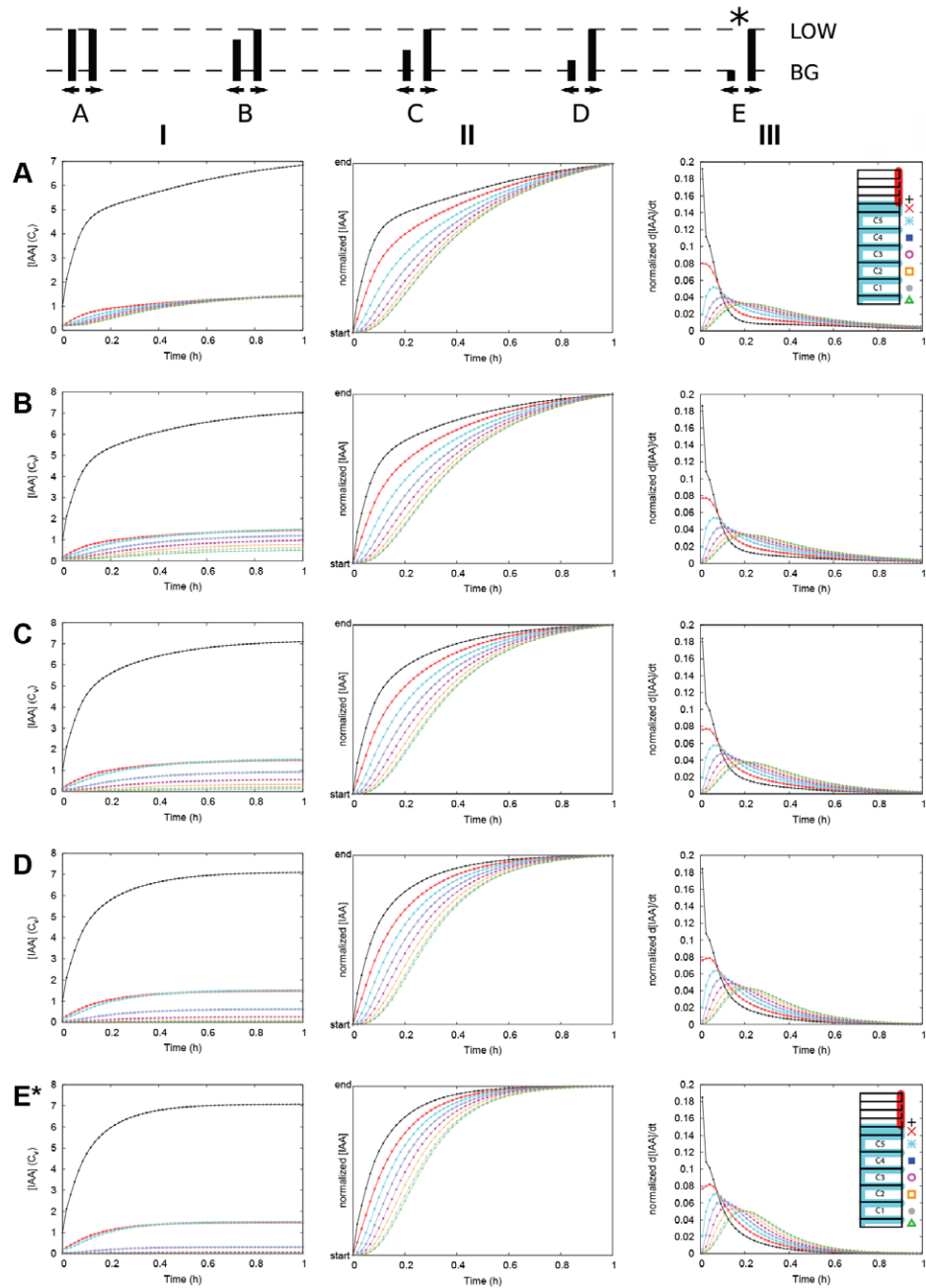
Fig. S6. Auxin accumulation always starts from the interior layers, regardless of inward: outward PIN bias in the cortex.

The amount of PIN (P_{eff}) before efflux reduction in the abaxial membrane of the cortical cells decreases from A, with P_{eff}=5 μm s^{-1} ("low") for abaxial and adaxial cell faces, to E, with P_{eff}=1 μm s^{-1} ("bg") for the abaxial cell face. This is illustrated in the cartoon on top. The root from Fig. 13, E in this figure, is marked with an asterisk (*). The full PIN distribution pattern is illustrated for A and E similar to Fig. 13B. This also shows the markers for the different cell layers. I: Concentration in the controlled area from the moment of efflux reduction (c.f. Fig. 13F). II: Concentration, rescaled from the initial value to the concentration at the end of the simulation (T=1 h; c.f. Fig. 13G). III: Concentration change. This is the time derivative of II, expressed in rescaled concentration units per minute (c.f. Fig. 13H). In all cases (A-E) the same relative order occurs: the first, strongest and fastest increase occurs in the pericycle, followed by endodermis, C5, etc. towards outer layers. The stronger the inward bias of the cortical PINs, the lower the steady state concentrations reached in the exterior root layers epidermis and outer cortex. It is likely that with a strong inward bias, i.e., towards the bottom of the figure, the maximum concentration reached in the outer cortex is insufficient to trigger a cell division response.

Movie 1. Concentration heat maps of the middle part of the root segment including the controlled area.